PCCP

PAPER

View Article Online
View Journal

Cite this: DOI: 10.1039/c7cp05850k

Ab initio and transition state theory study of the OH + HO_2 → H_2O + $O_2(^3\Sigma_g^-)$/$O_2(^1\Delta_g)$ reactions: yield and role of $O_2(^1\Delta_g)$ in H_2O_2 decomposition and in combustion of H_2†

M. Monge-Palacios *[ab] and S. Mani Sarathy [a]

Received 27th August 2017,
Accepted 19th January 2018

DOI: 10.1039/c7cp05850k

rsc.li/pccp

Reactions of hydroxyl (OH) and hydroperoxyl (HO_2) are important for governing the reactivity of combustion systems. We performed post-CCSD(T) *ab initio* calculations at the W3X-L//CCSD = FC/cc-pVTZ level to explore the triplet ground-state and singlet excited-state potential energy surfaces of the OH + HO_2 → H_2O + $O_2(^3\Sigma_g^-)$/$O_2(^1\Delta_g)$ reactions. Using microcanonical and multistructural canonical transition state theories, we calculated the rate constant for the triplet and singlet channels over the temperature range 200–2500 K, represented by $k(T) = 3.08 \times 10^{12} T^{0.07} \exp(1151/RT) + 8.00 \times 10^{12} T^{0.32} \exp(-6896/RT)$ and $k(T) = 2.14 \times 10^{6} T^{1.65} \exp(-2180/RT)$ in $cm^3\ mol^{-1}\ s^{-1}$, respectively. The branching ratios show that the yield of singlet excited oxygen is small (<0.5% below 1000 K). To ascertain the importance of singlet oxygen channel, our new kinetic information was implemented into the kinetic model for hydrogen combustion recently updated by Konnov (*Combust. Flame*, 2015, **162**, 3755–3772). The updated kinetic model was used to perform H_2O_2 thermal decomposition simulations for comparison against shock tube experiments performed by Hong *et al.* (*Proc. Combust. Inst.*, 2013, **34**, 565–571), and to estimate flame speeds and ignition delay times in H_2 mixtures. The simulation predicted a larger amount of $O_2(^1\Delta_g)$ in H_2O_2 decomposition than that predicted by Konnov's original model. These differences in the $O_2(^1\Delta_g)$ yield are due to the use of a higher *ab initio* level and a more sophisticated methodology to compute the rate constant than those used in previous studies, thereby predicting a significantly larger rate constant. No effect was observed on the rate of the H_2O_2 decomposition and on the flame speeds and ignition delay times of different H_2–oxidizer mixtures. However, if the oxidizer is seeded with O_3, small differences appear in the flame speed. Given that $O_2(^1\Delta_g)$ is much more reactive than $O_2(^3\Sigma_g^-)$, we do not preclude an effect of the singlet channel of the titled reaction in other combustion systems, especially in systems where excited oxygen plays an important role.

I. Introduction

Hydrogen combustion is the simplest combustion problem and a potential source of clean energy. Despite the large number of theoretical and experimental works carried out to understand its chemistry and physics, new reactions involved in the system H_2–O_2 are still being reported,[1] and some uncertainties on previously reported reactions still remain.

This is the case of the hydrogen abstraction reaction OH + HO_2 → H_2O + O_2, which can take place on two different potential energy surfaces (PESs). The barrier-less reaction

$$OH + HO_2 \rightarrow H_2O + O_2(^3\Sigma_g^-) \quad (R1)$$

occurs on the triplet ground-state PES and produces stable molecules, and thus is a chain termination reaction. There have been several theoretical and experimental studies to determine the rate of the reaction, with a particular emphasis on the temperature dependence. These two radicals can also react on the singlet excited-state PES,

$$OH + HO_2 \rightarrow H_2O + O_2(^1\Delta_g) \quad (R2)$$

producing singlet excited oxygen, which is much more reactive than the ground state oxygen formed in reaction (R1). To the best of our knowledge, only one theoretical kinetic study has

[a] King Abdullah University of Science and Technology, Clean Combustion Research Center, Thuwal 23955-6900, Saudi Arabia.
E-mail: manuel.mongepalacios@kaust.edu.sa, mani.sarathy@kaust.edu.sa
[b] University of Missouri-Columbia, Department of Chemistry, Columbia, MO 65211-7600, USA

† Electronic supplementary information (ESI) available. See DOI: 10.1039/c7cp05850k

been reported for reaction (R2) by González *et al.*,[2] using the conventional transition state theory with Wigner correction for tunneling based on MP4/6-31G** *ab initio* calculations.

Despite numerous theoretical and experimental studies on the reaction (R1), it has not been until recently that the magnitude and temperature dependence of its rate constant has been clarified. This motivates similar sophisticated studies to cast light on reaction (R2).

As for the reaction OH + HO_2 → H_2O + $O_2(^3\Sigma_g^-)$, Mozurkewich[3] performed a RRKM (Rice–Ramsperger–Kassel–Marcus) study on the fate of the complex HO_2OH, and reported a rate constant value of 6.5×10^{-11} cm^3 molecule^{-1} s^{-1} at 298 K for the formation of H_2O + $O_2(^3\Sigma_g^-)$ and a negative temperature dependence over the 250–450 K range. Toohey and Anderson[4] calculated a classical barrier height, $\Delta V^{\neq}$, of 2.5 kcal mol^{-1} at the UMP2/6-31G** *ab initio* level, but suggested that a saddle point with an energy below that of the reactants might explain the magnitude and the temperature dependence of the rate constant reported by Mozurkewich.[3]

González *et al.*[2,5] calculated the rate constant for the reactions (R1) and (R2), concluding that the reaction on the singlet PES is negligible, due to its large barrier height ($\Delta V^{\neq}$ = 14.4 kcal mol^{-1} at the MP4/6-31G** level). They found two saddle points on the triplet PES, one with a planar configuration and one with a non-planar configuration with classical energy barriers at the MP4/6-31G** *ab initio* level of 1.67 kcal mol^{-1} and 2.18 kcal mol^{-1}, respectively. Using these barrier heights, they obtained transition state theory rate constants for the triplet channel that are smaller than the experimental values reported by Keyser[6] for the 254–382 K temperature range. They pointed out that better *ab initio* methods are necessary for accurate predictions of the energy barrier to reaction (R1). In fact, an arbitrary reduction of the energy of the non-planar saddle point to −5.8 kcal mol^{-1}, with respect to the reactants, leads to agreement between their results and experiment. They predicted a barrier-less reaction in accord with Toohey and Anderson's[4] suggestion.

Recently, Burke *et al.*[7] used a multi-scale modeling approach (implemented for the H_2O_2 decomposition system) to determine the temperature dependence of the rate constant of OH + HO_2 → H_2O + $O_2(^3\Sigma_g^-)$. In their study, they incorporated for the reaction OH + HO_2 → H_2O + $O_2(^3\Sigma_g^-)$ *ab initio* information calculated at the MS-CASPT2/CBS//MS-CASPT2/aug-cc-pVTZ level and rate constants obtained with the two-transition-state model.[8,9] Other reactions important in H_2O_2 decomposition were also included in the model. They obtained the following two-term Arrhenius expression (in cm^3 mol^{-1} s^{-1}) for OH + HO_2 → H_2O + $O_2(^3\Sigma_g^-)$ for the temperature range 200–3000 K

$$k(T) = 1.93 \times 10^{20} T^{-2.49} \exp(-294/T) + 1.21 \times 10^{9} T^{1.24} \exp(658/T) \quad (1)$$

which gives k(298 K) = 1.0×10^{-10} cm^3 molecule^{-1} s^{-1} and k(2000 K) = 3.6×10^{-11} cm^3 molecule^{-1} s^{-1}. The agreement with González *et al.*[5] is good at high temperatures but not at the low temperatures. Eqn (1) shows a much more significant influence of temperature, and both sets of data disagree at temperatures between 298 K and 2000 K. Burke *et al.* predicted a minimum in the rate constant at 1125 K.

Pioneering experimental studies[6,10] of reaction (R1) showed weak and negative temperature dependence at low temperatures (252–420 K). Shock tube studies by Hippler *et al.*[11] and Kappel *et al.*[12] showed strong and non-Arrhenius temperature dependence at high temperatures, 1100–1600 K and 950–1250 K, respectively; with a minimum at 1250 K and 1100 K, respectively. Both proposed a complex mechanism involving bound intermediate complexes to explain their observations. However, Srinivasan *et al.*[13] and Hong *et al.*[14] observed weak temperature dependence over the 1200–1700 K and 1600–2200 K ranges, respectively, and could not confirm the existence of a minimum.

Hong *et al.*[15] recently improved upon their previous study, which was based on laser absorption of H_2O and OH, by considering the HO_2 absorption as well. By combining the results of their two studies, which cover the temperature range 1072–2200 K,[14,15] with those from other experiments[6,10,16–19] over the range 298–420 K, they proposed the following two-term Arrhenius expression (in cm^3 mol^{-1} s^{-1}) for the temperature range, 250–4000 K

$$k(T) = 7.0 \times 10^{12} \exp(550/T) + 4.5 \times 10^{14} \exp(-5500/T) \quad (2)$$

This is in good agreement with the theoretical results reported by Burke *et al.*[7] Only Hong *et al.*[15] and Burke *et al.*[7] have reported rate constants over a wide enough temperature range to clearly show the two different regions of the Arrhenius plot.

Consequently, the most recent kinetic models for hydrogen combustion, as the one recently updated by Konnov,[20] include Hong's[15] rate constant for the reaction OH + HO_2 → H_2O + $O_2(^3\Sigma_g^-)$, that is, eqn (2), and González's[2] rate constant for the reaction OH + HO_2 → H_2O + $O_2(^1\Delta_g)$, given by

$$k(T) = 1.1 \times 10^{5} T^{1.71} \exp(12\,535/RT) \quad (3)$$

In this work, we performed high-level electronic structure and variational transition state theory calculations over the temperature range 200–2500 K. The goals were to accurately characterize the saddle points on the triplet ground-state and singlet excited-state PESs of the reactions OH + HO_2 → H_2O + $O_2(^3\Sigma_g^-)$/ $O_2(^1\Delta_g)$ to determine their rate constant over a wide temperature range. Special attention was devoted to the excited channel, for which the current accepted rate constant is based on low level *ab initio* and kinetic calculations. We also shed light on the anomalous temperature dependence of the rate constant of OH + HO_2 → H_2O + $O_2(^3\Sigma_g^-)$ and calculated branching ratios to OH + HO_2 → H_2O + $O_2(^1\Delta_g)$. With this kinetic information we updated Konnov's kinetic model and performed simulations using CHEMKIN-PRO,[21] determining the yield of $O_2(^1\Delta_g)$ and its role in the H_2O_2 thermal decomposition and in the combustion of H_2.

II. Computational methods

II.1. *Ab initio* calculations

The singlet excited-state and triplet ground-state PESs for OH + HO_2 → H_2O + O_2 were explored by performing post-CCSD(T)

ab initio electronic structure calculations using the Gaussian 09,[22] Molpro[23] and MRCC[24] packages, at the W3X-L//CCSD = FC/cc-pVTZ level. The geometry optimizations and frequency calculations were done using the CCSD = FC coupled-cluster method[25] with the cc-pVTZ basis set[26] with Gaussian09. The energy was refined by using the W3X-L composite method[27] with Molpro and MRCC, which has been proven to be efficient for estimating CCSDT(Q)/CBS energies and handeling problems with moderate multireference character.

We also calculated the minimum energy path (MEP) of both reactions over the range −2.0 Bohr to +2.0 Bohr of the reaction coordinate s with step size 0.05 Bohr in mass-scaled coordinates with a scaling mass equal to 1 amu. The Hessian was evaluated every third step. The MEP was calculated using the Gaussrate code,[28] which is an interface between the Gaussian 03 package[29] and Polyrate 9.5.[30]

II.2. Rate constant calculations

The rate constant calculations were carried out using the polyatomic rate constant codes Polyrate 9.5[30] and Polyrate 2016-2A.[31] MSTor code[32] was used to account for multistructural anharmonicity.

We performed a normal mode analysis along the MEP, calculating the ground-state vibrationally adiabatic potential energy curve

$$V_a^G(s) = V_{MEP}(s) + ZPE(s) \quad (4)$$

where $V_{MEP}(s)$ is the classical potential energy and ZPE(s) is the zero-point energy at s.

The thermal rates for the reaction OH + HO_2 → H_2O + $O_2(^3\Sigma_g^-)$ were estimated using the microcanonical variational theory (μVT),[33] in which the "best" dividing surface is variationally determined at each total energy, E; the dividing surface $s_{\mu VT}$* is that surface where the sum of vibrational–rotational states of the transition state N_{vr}*(E) is a minimum. The microcanonical rate constant is given by

$$k_{\mu VT}(E) = \frac{N_{vr}{}^*(E)}{h\phi^R(E)} \quad (5)$$

where $\phi^R(E)$ is the reactants density of states per unit energy and volume. The thermal rate constant is obtained from $k_{\mu VT}(E)$ and the Boltzmann distribution $P(E)$

$$k(T) = \sigma\int_0^\infty k_{\mu VT}(E)P(E)dE \quad (6)$$

The factor σ is the number of equivalent reaction paths; that is, the reaction degeneracy,[34] calculated with the rotational symmetry numbers of the reactants $\sigma_{rot,OH}$ and σ_{rot,HO_2}, and transition state $\sigma_{rot,TS}$ (see SP1(^{3}A) in Fig. 1),

$$\sigma = \frac{\sigma_{rot,OH}\cdot\sigma_{rot,HO_2}}{\sigma_{rot,TS}} \quad (7)$$

Since the rotational symmetry number is one for the three species in OH + HO_2 → H_2O + $O_2(^3\Sigma_g^-)$, the reaction degeneracy is one. However, due to the non-planar geometry of the saddle point on the triplet PES (see SP1(^{3}A) in Fig. 1), we should also consider a non-superimposed structure that corresponds to an equivalent transition state. Therefore, although the reaction degeneracy is one, the total rate constant for OH + HO_2 → H_2O + $O_2(^3\Sigma_g^-)$ should be multiplied by two.[34]

The rate constants for the reaction OH + HO_2 → H_2O + $O_2(^1\Delta_g)$ were computed by employing the multistructural[35–37] canonical transition state theory[38,39] including torsional anharmonicity

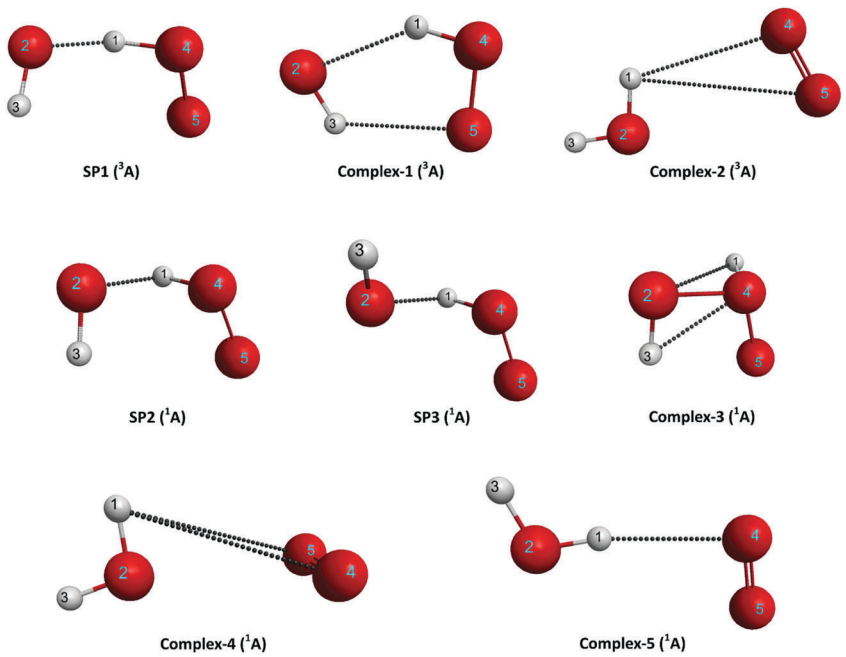

Fig. 1 Optimized structures of the saddle points and intermediate complexes (also see Table 1) on the low-lying triplet ground-state (^{3}A) and singlet excited-state (^{1}A) PESs of the reaction OH + HO_2 → H_2O + O_2 at the CCSD = FC/cc-pVTZ level. The oxygen and hydrogen atoms are shown, respectively, in red and white.

with a coupled torsional potential, MS-T(C). In this version of the transition state theory, the conformational rotational–vibrational partition function of each stationary point is defined as

$$Q_{\text{con-rovib}}^{\text{MS-T(C)}} = \sum_{j=1}^{J} Q_{\text{rot},j} \exp(-\beta U_j) Q_j^{\text{HO}} \prod_{\eta=1}^{t} \bar{f}_{j,\eta} \qquad (8)$$

where the summation runs over the set of conformers J. $Q_{\text{rot},j}$ is the classical rotational partition function, β is $1/k_{\text{B}}T$, U_j is the energy defined with respect to the global minimum structure, set to j = 1, and Q_j^{HO} is the normal-mode harmonic oscillator partition function; the term $\bar{f}_{j,\eta}$ is used to introduce the torsional anharmonicity associated to the coupled torsion η by adjusting the partition function Q_j^{HO}. One of the advantages of the vibrational partition function defined by eqn (8) is that there is no need to assign the torsional motions to specific normal modes.

The single structural rotational–vibrational partition function for the conformer j, $Q_{\text{con-rovib},j}^{\text{SS-T(C)}}$, including torsional anharmonicity and coupled torsions is defined as

$$Q_{\text{con-rovib},j}^{\text{SS-T(C)}} = Q_{\text{rot},j} \exp(-\beta U_j) Q_j^{\text{HO}} \prod_{\eta=1}^{t} \bar{f}_{j,\eta} \qquad (9)$$

The partition function Q_j^{HO}, used in eqn (8) and (9), is given by

$$Q_j^{\text{HO}} = \exp(-h\omega/2k_{\text{B}}T)[1 - \exp(-h\omega/k_{\text{B}}T)]^{-1} \qquad (10)$$

The multistructural torsional anharmonicity factor $F_{\text{X}}^{\text{MS-T(C)}}$ is defined for the minima (reactants, $F_{\text{R}}^{\text{MS-T(C)}}$) and saddle points ($F_{\neq}^{\text{MS-T(C)}}$) as

$$F_{\text{X}}^{\text{MS-T(C)}} = Q_{\text{con-rovib}}^{\text{MS-T(C)}} / Q_{\text{con-rovib},j=1}^{\text{SS-T(C)}} \qquad (11)$$

This factor is also defined for the reaction as

$$F^{\text{MS-T(C)}} = F_{\neq}^{\text{MS-T(C)}} / F_{\text{R}}^{\text{MS-T(C)}} \qquad (12)$$

The electronically excited-state $^2\Pi_{1/2}$ of the reactant OH, which lies 140 cm^{-1} ($\approx$0.4 kcal mol^{-1}) over the $^2\Pi_{3/2}$ ground-state, was included in the calculation of its electronic partition function, Q_{elec}, in both reactions, OH + HO_2 → H_2O + $O_2(^3\Sigma_g^-)$/$O_2(^1\Delta_g)$. The first electronically excited state of HO_2, ^{2}A′, lies about 20.3 kcal mol^{-1} above the ground state, ^{2}A″.[40,41] So, we assumed that the HO_2 radical has a significant population in the ground state, not including the ^{2}A′ excited state in the reactants electronic partition functions.

The frequencies were scaled by a factor of 0.941[42] for a better description of the torsional anharmonicity as well as to obtain a more accurate $V_{\text{a}}^{\text{G}}(s)$ curve. To account for the quantum effects on the reaction coordinate of both reactions, we used the small-curvature tunneling (SCT)[30,43] approach, obtaining the transmission coefficients κ^{SCT}.

The final rate constant for the reaction OH + HO_2 → H_2O + $O_2(^1\Delta_g)$ is calculated as

$$k_{\text{MS-T(C)}}^{\text{CVT/SCT}} = \kappa^{\text{SCT}} \Gamma \frac{k_{\text{B}}T}{h} \frac{Q_{\text{elec}}^{\neq} Q_{\text{con-rovib}}^{\text{MS-T(C)},\neq}}{\Phi_{\text{t}} Q_{\text{elec}}^{\text{R}} Q_{\text{con-rovib}}^{\text{MS-T(C)},\text{R}}} \exp(-\beta V^{\neq}) \qquad (13)$$

where the superscripts $\neq$ and R stand for conventional transition state and reactants, respectively. Since the reactants OH and HO_2 do not have torsional motions and thus multiple conformers, $Q_{\text{con-rovib}}^{\text{MS-T(C)},\text{R}}$ is equivalent to the single structure partition function. The factor Γ is the recrossing transmission coefficient, given by the ratio of the CVT rate constant to the TST one. Both, κ^{SCT} and Γ terms, are calculated using the global minimum structure and the harmonic oscillator approach.

II.3. Numerical simulations of the H_2O_2 decomposition

The H_2O_2 thermal decomposition experiment carried out by Hong *et al.*[15] behind reflected shock waves was simulated in CHEMKIN-PRO[21] using a closed homogenous batch reactor and Konnov's kinetic model[20] with the kinetic information obtained in this work for the reactions OH + HO_2 → H_2O + $O_2(^3\Sigma_g^-)$ and OH + HO_2 → H_2O + $O_2(^1\Delta_g)$.

The initial conditions were the same as those in Hong's experiment, that is, initial gas temperature and pressure of 1182 K and 1.672 atm, respectively. The initial composition of the bulk was also defined as in Hong's experiment: 0.996285 Ar, 0.001113 H_2O, 0.002046 H_2O_2 and 0.000556 $O_2(^3\Sigma_g^-)$ (in mole fraction). We used the default value of 1 cm^3 for the initial volume, and the ending time for the simulation was set to 0.1 s.

Additional simulations were run using the same initial conditions but at different temperatures of 1000 K, 1500 K and 1800 K, with the goal of analyzing the effect of our updated rates on H_2O_2 decomposition at various conditions.

We have also estimated flame speeds and ignition delays in different H_2 mixtures using a premixed laminar flame-speed simulator (ambient temperature and initial gas pressure of 300 K and 1 atm, respectively) and a closed homogeneous batch reactor, respectively. For the flame speeds we used three different oxidizers: air, air seeded with $O_2(^1\Delta_g)$, that is, 22.18% $O_2(^3\Sigma_g^-)$ + 1.11% $O_2(^1\Delta_g)$ + 76.71% N_2, and $O_2(^3\Sigma_g^-)$ seeded with O_3, that is, 60.9% $O_2(^3\Sigma_g^-)$ + 39.1% O_3, at different equivalent ratios. As for the ignition delay times simulations, a mixture of 0.81% H_2 + 4.03% $O_2(^3\Sigma_g^-)$ + Ar was used, testing different initial gas pressures, 1 bar, 4 bar and 16 bar, at temperatures between 900 K and 2000 K.

III. Results and discussion

III.1. Topology of the triplet and singlet potential energy surfaces

The reactions OH + HO_2 → H_2O + $O_2(^3\Sigma_g^-)$/$O_2(^1\Delta_g)$ can proceed through several intermediate complexes and saddle points. While the triplet channel is correlated to the ground-state products, H_2O + $O_2(^3\Sigma_g^-)$, the singlet channel leads to the excited-state products, H_2O + $O_2(^1\Delta_g)$. Table 1 lists the optimized geometric parameters, harmonic vibrational frequencies, energy, and enthalpy at 0 K defined with respect to the reactants OH + HO_2 computed at the W3X-L//CCSD = FC/cc-pVTZ *ab initio* level for the intermediate complexes and saddle points located on both PESs. The optimized structures are shown on Fig. 1.

On the triplet ground-state PES, two intermediate complexes were optimized and characterized: a hydrogen-bonded complex in the entry channel, Complex-1(^{3}A), and another in the

Table 1 *Ab initio* properties of the stationary points[a] on the low-lying triplet ground-state (^{3}A) and singlet excited-state (^{1}A) PESs at the W3X-L//CCSD = FC/cc-pVTZ level[b]

	Geometry	Frequencies	ΔV	ΔH (0 K)
SP1(^{3}A)				
rO(4)–H(1)	1.039	3775, 1543, 1469	−2.38	−3.45
rO(2)–H(1)	1.393	1146, 663, 477		
αO(2)–H(1)–O(4)	161.7	212, 104, 2105i		
βO(5)–O(4)–H(1)–O(2)	76.6			
βH(3)–O(2)–H(1)–O(4)	−35.6			
Complex-1(^{3}A)				
rO(2)–H(1)	1.959	3709, 3597, 1548	−3.21	−0.98
rO(5)–H(3)	2.211	1193, 513, 468		
βO(5)–O(4)–H(1)–O(2)	−0.3	286, 213, 164		
βH(3)–O(2)–H(1)–O(4)	0.3			
Complex-2(^{3}A)[c]				
rO(4)–H(1)	2.642	3981, 3877, 1677	−70.33	−68.29
rO(5)–H(1)	3.418	1669, 91, 85		
βO(5)–O(4)–H(1)–O(2)	0.1	78, 64, 43		
SP2(^{1}A)				
rO(4)–H(1)	1.008	3825, 3090, 1465	0.23	2.31
rO(2)–H(1)	1.505	1289, 870, 502		
αO(2)–H(1)–O(4)	100.8	298, 260, 1012i		
βO(5)–O(4)–H(1)–O(2)	107.0			
βH(3)–O(2)–H(1)–O(4)	−64.6			
SP3(^{1}A)				
rO(4)–H(1)	1.006	3843, 3134, 1411	0.16	2.23
rO(2)–H(1)	1.516	1307, 816, 498		
αO(2)–H(1)–O(4)	100.3	306, 272, 1005i		
βO(5)–O(4)–H(1)–O(2)	105.4			
βH(3)–O(2)–H(1)–O(4)	58.5			
Complex-3(^{1}A)				
rO(2)–O(4)	1.481	3717, 3665, 1464, 1269	8.14	12.93
βO(5)–O(4)–O(2)–H(3)	4.1	1086, 853, 660, 416, 360		
Complex-4(^{1}A)				
rO(4)–H(1)	3.177	3979, 3876, 1678, 1599	−47.53	−45.60
rO(5)–H(1)	3.100	95, 94, 87, 60, 8		
Complex-5(^{1}A)				
rO(4)–H(1)	2.238	3975, 3875, 1687	−47.71	−45.48
rO(5)–H(1)	2.771	1597, 196, 164		
βO(2)–H(1)–O(4)–O(5)	10.2	115, 49, 40		

[a] The notations are defined in Fig. 1. [b] Distances are in angstroms, angles in degrees, frequencies in cm^{-1} and energies and enthalpies in kcal mol^{-1}. [c] Complex-2(^{3}A) is reported at the CCSD(T) = FC/cc-pVTZ//CCSD = FC/cc-pVTZ level due to convergence problems with the W3X-L level.

exit channel, Complex-2(^{3}A), due to dipole-induced dipole interactions between the polar H_2O and the non-polar O_2. Complex-1(^{3}A) is accommodated by a well that is −3.21 kcal mol^{-1}, with respect to the reactants. This complex has been previously reported. Jackels and Phillips[44] optimized it using the CI(SDQ) method and a polarized double-ζ basis set, obtaining an energy of −5.3 kcal mol^{-1}. González *et al.*[5] reported values ranging from −4.2 kcal mol^{-1} to −9.6 kcal mol^{-1} at different single point levels based on HF/6-31G** and MP2/6-31** optimized structures. Zhang *et al.*[45] using the CCSD(T) = FC/aug-cc-pVTZ//CCSD = FC/6-311G(d,p) level obtained −8.0 kcal mol^{-1}. We attribute these differences to the more robust method used in our calculations.

The W3X-L method failed to obtain the energy of Complex-2(^{3}A) due to convergence problems; its CCSD(T) = FC/cc-pVTZ//CCSD = FC/cc-pVTZ energy is only 0.9 kcal mol^{-1} below that of the products H_2O + $O_2(^3\Sigma_g^-)$ at the same level, as a result of the weak dipole-induced dipole and dispersion interactions between the polar H_2O and the non-polar $O_2(^3\Sigma_g^-)$ molecules. To the best of our knowledge, Complex-2(^{3}A) has not been reported.

We also found a non-planar saddle point on the triplet PES, which we label SP1(^{3}A). The imaginary frequency is 2105 cm^{-1}. The classical and adiabatic energies are −2.38 kcal mol^{-1} and −3.45 kcal mol^{-1}, respectively, with respect to the reactants. The classical barriers reported by González *et al.*[5] for this saddle point are 18.82 kcal mol^{-1} and 2.89 kcal mol^{-1}, respectively, at the HF/6-31G** and MP2/6-31** levels. Using the CCSD(T) = FC/aug-cc-pVTZ//CCSD = FC/6-311G(d,p) level, Zhang *et al.*[45] obtained classical and adiabatic barrier heights of 0.5 kcal mol^{-1} and −0.62 kcal mol^{-1}, respectively. This illustrates that the barrier height of this system is very sensitive to

the *ab initio* level used, which in part accounts for the large differences in the theoretical values of $k(T)$ in literature. We also attribute these differences to the more sophisticated *ab initio* method used in this work.

One intermediate complex in the entry channel, Complex-3(^{1}A), and two intermediate complexes in the exit channel, Complex-4(^{1}A) and Complex-5(^{1}A), were optimized and characterized for the singlet excited-state PES. Zhang *et al.*[45] obtained an energy value of 9.1 kcal mol^{-1} for Complex-3(^{1}A), which is 1.0 kcal mol^{-1} larger than that obtained in this work. The intermediates Complex-4(^{1}A) and Complex-5(^{1}A) are formed as a consequence of the dipole-induced dipole and dispersion interactions, being weakly bonded with respect to the products $H_2O + O_2(^1\Delta_g)$, with classical energies of -0.26 kcal mol^{-1} and -0.44 kcal mol^{-1}, respectively.

Two saddle points were identified on the singlet excited-state PES, SP2(^{1}A) and SP3(^{1}A), with imaginary frequencies of 1012 cm^{-1} and 1005 cm^{-1}, respectively. The classical and adiabatic barrier heights are also similar, 0.23 kcal mol^{-1} and 2.31 kcal mol^{-1} for SP2(^{1}A) and 0.16 kcal mol^{-1} and 2.23 kcal mol^{-1} for SP3(^{1}A), respectively. Zhang *et al.*[45] also found these two saddle points, with classical energies of 3.0 kcal mol^{-1}.

We verified that there are no more saddle points on the studied low-lying triplet and singlet PESs by exploring the conformational space of the structures SP1(^{3}A), SP2(^{1}A) and SP3(^{1}A). The dihedrals H(3)–O(2)–H(1)–O(4) and O(2)–H(1)–O(4)–O(5) were rotated by 120° and all the possible combinations of these two angles were optimized. Only SP1(^{3}A), SP2(^{1}A), SP3(^{1}A) and their mirror image pairs were optimized and characterized as addle points. These structures are non-superimposable mirror images connected by internal rotations, thus all of them were considered in the kinetic calculations.

Fig. 2 shows the classical potential energy profiles for $OH + HO_2 \rightarrow H_2O + O_2(^3\Sigma_g^-)$ and $OH + HO_2 \rightarrow H_2O + O_2(^1\Delta_g)$ computed at the W3X-L//CCSD = FC/cc-pVTZ *ab initio* level. The difference in the barrier heights of the triplet ground-state and singlet excited-state PESs is -2.54 kcal mol^{-1} and -5.68 kcal mol^{-1} for the classical and adiabatic barriers, respectively. While the reaction on the triplet PES is energetically favored, the difference in the barrier heights are not large enough to completely preclude the $OH + HO_2 \rightarrow H_2O + O_2(^1\Delta_g)$ reaction at the high temperatures reached in combustion. This reaction could serve as a source of $O_2(^1\Delta_g)$, which can play a role in hydrogen combustion under certain conditions, as has been demonstrated theoretically[46] and experimentally,[47–50] since it is much more reactive than ground-state oxygen.

Given that the electronic transition from the triplet to the singlet electronic state implies a change in the total spin angular momentum, we expect that transition to be forbidden or unlikely probable. Electronic triplet → singlet transitions have been reported as probable for other reactive systems in which both PESs cross in the proximity of a bound intermediate. This is the case of the reaction $O_2 + C_2H_4$ studied by Park *et al.*,[51] who reported a possible enhancement of that transition due to a trapping in the well of an intermediate complex of the triplet PES. However, due to the larger energy gap between the two PESs studied in this work, which do not show any crossing point, we do not expect the intermediate Complex-1(^{3}A) to promote a triplet → singlet transition.

We will use the shock tubes rate constants measurements by Hong *et al.*[15] as a test to our electronic structure and kinetic calculations. As an additional test to the level of theory used in our calculations, we compare the enthalpy of reaction at 0 K

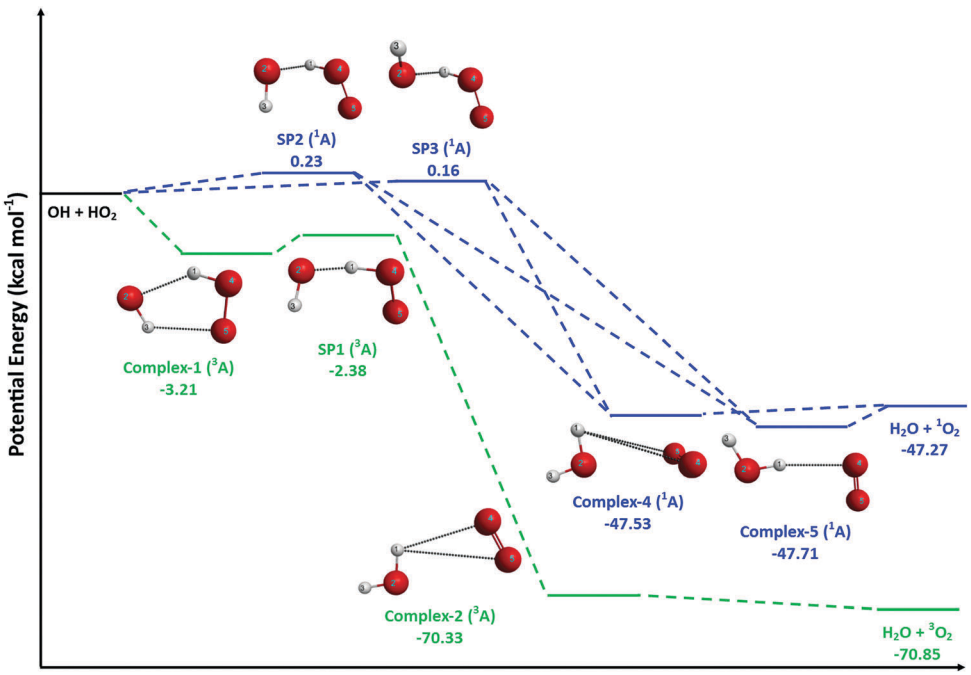

Fig. 2 Classical potential energy profile at the W3X-L//CCSD = FC/cc-pVTZ level in kcal mol^{-1} for the low-lying triplet ground-state (green) and singlet excited-state (blue) PESs. The energies of the stationary points are defined with respect to those of the reactants.

obtained in our work for the OH + HO_2 → H_2O + $O_2(^3\Sigma_g^-)$ channel, $\Delta H_R^\circ(0\ K) = -69.3$ kcal mol^{-1}, to the value obtained from the Active Thermochemical Tables (ATcT) approach,[52–54] $\Delta H_R^\circ(0\ K) = -69.6$ kcal mol^{-1}. These tables include a more accurate value of the enthalpy of formation of the HO_2 radical, for which large uncertainties exist, obtaining a more accurate value of $\Delta H_R^\circ(0\ K)$ than the one given in the JANAF Tables,[55] −67.6 kcal mol^{-1}. Our result differs from the experimental value by only 0.3 kcal mol^{-1}. As for the reaction OH + HO_2 → H_2O + $O_2(^1\Delta_g)$, we obtained $\Delta H_R^\circ(0\ K) = -45.9$ kcal mol^{-1}, also in good agreement with the value from ATcT, −47.1 kcal mol^{-1}.

III.2. Rate constants

(a) Reaction on the triplet PES. We used the microcanonical variational transition-state theory to calculate the rate constant for the reaction OH + HO_2 → H_2O + $O_2(^3\Sigma_g^-)$ at temperatures between 200 K and 2500 K (dark blue curve in Fig. 3) using information from the electronic structure calculations at the W3X-L//CCSD = FC/cc-pVTZ level. Fig. 3 shows the Arrhenius plots of the experimental and theoretical values of the rate constant available in literature, as well as ours, for OH + HO_2 → H_2O + $O_2(^3\Sigma_g^-)$ over the temperature range 200–4000 K for comparison.

González *et al.*[5] (green curve in Fig. 3) using the low level MP4/6-31G** predict essentially no influence of temperature, which is in disagreement with the other results in Fig. 3. Burke *et al.*[7] performed more accurate electronic structure calculations using the MS-CASPT2/CBS//MS-CASPT2/aug-cc-pVTZ *ab initio* level and predicted a strong influence of temperature on the rate constant (light blue curve in Fig. 3), with a negative dependence at temperatures below 1125 K. In agreement with the results by Burke *et al.*, we also predict a significant influence of temperature in the rate constant and a minimum in the Arrhenius plot, although at 850 K. The discrepancies among the rate constants by González *et al.*[5] and those by Burke *et al.*[7] and ours are due to the low *ab initio* method and basis set used by González *et al.* to determine the barrier height and the different methods used to calculate the rate constants; despite the low level *ab initio* method used by González *et al.* 25 years ago, their results are approximately within an order of magnitude to the more recent calculations reported by Burke *et al.* and by us.

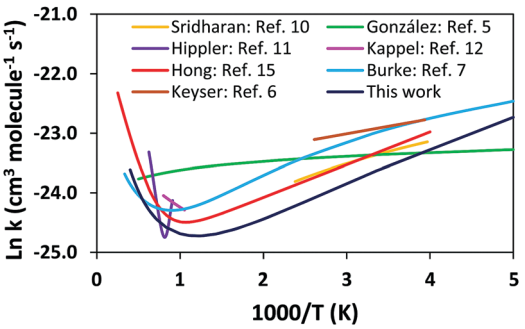

Fig. 3 Plots of ln k (cm^3 molecule^{-1} s^{-1}) *versus* 1000/T (K): experimental (ref. 6, 10, 11, 12 and 15) and theoretical (ref. 5, 7, and this work) results.

As for the experimental studies included in Fig. 3, only Hong *et al.*[15] and Hippler *et al.*[11] (red and purple curves, respectively, in Fig. 3) based on laser absorption and shock tubes experiments, respectively, cover wide enough temperature ranges to reveal the different behaviors of the rate constant at low and high temperatures; their results indicate a minimum at 925 K and 1250 K, respectively.

The Burke *et al.*[7] results and ours, based on high levels of theory, are the most accurate theoretical results available to date. The Hong *et al.*[15] experiments provide the critical data extending over the temperature range that includes the minimum in the rate constant for validation of the theoretical predictions. Thus, it is informative to examine in detail these three sets of results.

Table 2 lists the predicted values of the thermal forward rate constant for OH + HO_2 → H_2O + $O_2(^3\Sigma_g^-)$ over the temperature range 200–4000 K from ref. 7 (eqn (1)), ref. 15 (eqn (2)), and the present work. We fitted our rate constants to the following two-term Arrhenius expression (cm^3 mol^{-1} s^{-1}) over the 200–2500 K range:

$$k(T) = 3.08 \times 10^{12} T^{0.07} \exp(1151/RT) + 8.00 \times 10^{12} T^{0.32} \exp(-6896/RT) \quad (14)$$

Quantum effects on the reaction coordinate are not important (κ^{SCT} = 1 over the entire temperature range), as expected for a barrier-less reaction. Our results (dark blue curve in Fig. 3) are in good agreement with the experiments (red curve in Fig. 3), with similar predictions for the minimum (our: 850 K, Hong *et al.*'s: 925 K), and also with the values calculated by Burke *et al.*[7] (light blue curve in Fig. 3), who predict the minimum at 1125 K. We infer that the discrepancies between these two sets of calculated data are mainly due to the differences in the barrier heights predicted by the different levels of theory; Burke *et al.* did not report a value for the barrier height.

Table 2 Thermal rate constants (cm^3 molecule^{-1} s^{-1}) for the OH + HO_2 → H_2O + $O_2(^3\Sigma_g^-)$ reaction

T (K)	μVT[a]	Burke *et al.*[b]	Hong *et al.*[c]
200	1.34×10^{-10}	1.76×10^{-10}	
298	5.46×10^{-11}	1.04×10^{-10}	7.36×10^{-11}
400	3.25×10^{-11}	6.85×10^{-11}	4.60×10^{-11}
500	2.43×10^{-11}	5.05×10^{-11}	3.49×10^{-11}
600	2.06×10^{-11}	4.05×10^{-11}	2.91×10^{-11}
700	1.89×10^{-11}	3.47×10^{-11}	2.58×10^{-11}
800	1.83×10^{-11}	3.13×10^{-11}	2.39×10^{-11}
900	1.84×10^{-11}	2.94×10^{-11}	2.31×10^{-11}
1000	1.90×10^{-11}	2.85×10^{-11}	2.32×10^{-11}
1100	1.95×10^{-11}	2.81×10^{-11}	2.42×10^{-11}
1200	2.11×10^{-11}	2.83×10^{-11}	2.60×10^{-11}
1600	2.83×10^{-11}	3.13×10^{-11}	4.04×10^{-11}
2000	3.86×10^{-11}	3.63×10^{-11}	6.31×10^{-11}
2500	5.56×10^{-11}	4.37×10^{-11}	9.73×10^{-11}
3000		5.19×10^{-11}	1.33×10^{-10}
3500			1.69×10^{-10}
4000			2.02×10^{-10}

[a] This work, microcanonical variational transition state theory at the W3X-L//CCSD = FC/cc-pVTZ level. [b] Values calculated using eqn (1). Values are given only for the range over with eqn (1) was fit to data. [c] Values calculated using eqn (2).

In the 850–2500 K temperature range, the rate constant calculated in this work obeys the Arrhenius equation, but not at temperatures below 850 K. Non-Arrhenius temperature dependence has been observed for others barrier-less reactions with an intermediate complex in the entry channel.[56,57] The temperature dependence of the rate constant of the reaction OH + HO_2 → H_2O + $O_2(^3\Sigma_g^-)$ can be explained by analyzing the variation of the activation energy with temperature. In the absence of tunneling, the activation energy for a gas-phase bimolecular reaction is given by[58]

$$E_a = \Delta H^{\neq\circ} + 2RT \quad (15)$$

where $\Delta H^{\neq\circ}$ is the activation enthalpy. The activation energy to the reaction OH + HO_2 → H_2O + $O_2(^3\Sigma_g^-)$ is represented as function of temperature in Fig. 4, together with $\Delta H^{\neq\circ}$ and $2RT$. It can be seen that at temperatures higher than 850 K the activation energy is positive, resulting in a negative slope of the Arrhenius plot over the 850–2500 K range. However, at temperatures lower than 850 K, the positive term $2RT$ does not balance the activation enthalpy $\Delta H^{\neq\circ}$, which is negative in the whole temperature range. As a result, E_a becomes negative, and results in a positive slope of the Arrhenius representation, and then in a non-Arrhenius behavior. At 850 K the activation energy is zero, leading to a minimum in the rate constant at that temperature.

(b) Reaction on the singlet PES. We used the multistructural transition state theory with torsional anharmonicity and a coupled torsional potential, MS-T(C), as described in Section II.2, to compute the rate constants of the singlet channel, OH + HO_2 → H_2O + $O_2(^1\Delta_g)$. For the saddle points found on the singlet PES, SP2(^{1}A) and SP3(^{1}A), the dihedrals H(3)–O(2)–H(1)–O(4) and O(2)–H(1)–O(4)–O(5), τ_1 and τ_2, respectively, are strongly coupled, thus the Voronoi method, as implemented in MSTor,[32] was employed to estimate the periodicity parameters $M_{j,\tau}$ and carry out the partition function calculations. Thus, the scheme NS : SC = 0 : 2 was used, where NS and SC stand for nearly separable and strongly coupled.

The multistructural torsional anharmonicity factor $F^{\text{MS-T(C)}}$ (eqn (12)) of the reaction OH + HO_2 → H_2O + $O_2(^1\Delta_g)$ is shown in Table 3, together with the transmission coefficient, the rate constant (eqn (13)), and the branching ratio (BR) to the singlet channel, calculated as the ratio of the rate constant of the singlet channel to the sum of the rate constant of the singlet and triplet channels. The values calculated by González *et al.*[2] using the conventional transition state theory with Wigner correction for tunneling ($k^{\text{TST/W}}$) are also included for comparison. Since the reactants do not have conformers, $F_R^{\text{MS-T(C)}}$ is equal to 1, and thus $F^{\text{MS-T(C)}}$ reduces to $F_{\neq}^{\text{MS-T(C)}}$. The rate constant was fitted to the following Arrhenius expression (cm^3 mol^{-1} s^{-1}) over the 200–2500 K range

$$k(T) = 2.14 \times 10^6 T^{1.65} \exp(-2180/RT) \quad (16)$$

Table 3 Multistructural anharmonicity factor, SCT transmission coefficient, rate constant (cm^3 molecule^{-1} s^{-1}) and branching ratio (%) for the reaction OH + HO_2 → H_2O + $O_2(^1\Delta_g)$. The rate constant from ref. 2 (cm^3 molecule^{-1} s^{-1}) is also included for comparison

T (K)	$F^{\text{MS-T(C)}}$ [a]	κ^{SCT}	$k^{\text{CVT/SCT}}_{\text{MS-T(C)}}$ [a]	BR	$k^{\text{TST/W}}$ [b]
200	3.39	1.45	9.47×10^{-17}	7.07×10^{-5}	2.76×10^{-29}
298	3.49	1.18	1.07×10^{-15}	1.95×10^{-3}	
400	3.54	1.09	4.34×10^{-15}	1.33×10^{-2}	
500	3.56	1.06	1.08×10^{-14}	4.45×10^{-2}	2.58×10^{-20}
600	3.58	1.04	2.12×10^{-14}	1.03×10^{-1}	
700	3.59	1.03	3.61×10^{-14}	1.91×10^{-1}	
800	3.60	1.02	5.57×10^{-14}	3.03×10^{-1}	
900	3.61	1.02	8.04×10^{-14}	4.35×10^{-1}	
1000	3.62	1.01	1.10×10^{-13}	5.79×10^{-1}	3.76×10^{-17}
1100	3.64	1.01	1.46×10^{-13}	7.43×10^{-1}	
1200	3.65	1.01	1.84×10^{-13}	8.64×10^{-1}	
1600	3.68	1.01	3.42×10^{-13}	1.20 × 10	
2000	3.71	1.00	5.61×10^{-13}	1.43 × 10	3.73×10^{-15}
2500	3.74	1.00	9.26×10^{-13}	1.64 × 10	

[a] Our results, including torsional anharmonicity with a coupled torsional potential and tunneling using the SCT method. [b] Values from ref. 2, using conventional transition state theory and Wigner corrections for tunneling.

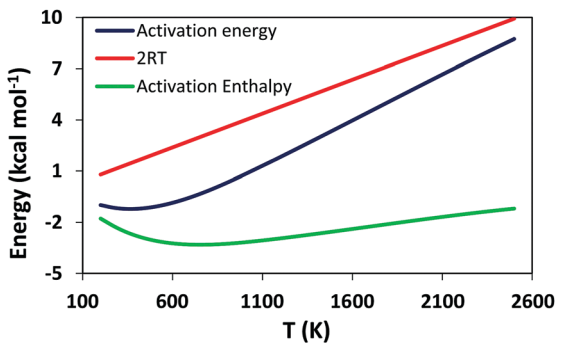

Fig. 4 Plots of the activation energy, activation enthalpy, and $2RT$ as functions of temperature.

It can be seen that the rate constant of the reaction OH + HO_2 → H_2O + $O_2(^1\Delta_g)$ is significantly smaller than that of the reaction OH + HO_2 → H_2O + $O_2(^3\Sigma_g^-)$ across the entire temperature range. As a result, the branching ratio to the singlet channel is also small, and high temperatures are necessary to produce a small amount of $O_2(^1\Delta_g)$. For instance, at temperatures as high as 2000 K, the yield of singlet excited oxygen is only 1.43%. The branching ratios suggest that the reaction OH + HO_2 → H_2O + $O_2(^1\Delta_g)$ is not competitive, being the reaction OH + HO_2 → H_2O + $O_2(^3\Sigma_g^-)$ dominant even at very high temperature. However, the role of the singlet excited oxygen formed in OH + HO_2 → H_2O + $O_2(^1\Delta_g)$ may not only depend on its yield, but also on its reactivity relative to that of the ground state oxygen. These issues are discussed in Section III.3.

Table 3 also shows that the rate constants reported by González *et al.*[2] are much smaller than those predicted in this work. Given that we are using higher levels of theory for the electronic structure calculations, as well as more sophisticated methods to estimate the rate constant and the tunneling contribution, we consider our results more accurate.

III.3. Role of the $O_2(^1\Delta_g)$ in H_2O_2 decomposition and in combustion of H_2–O_2 mixtures

We have carried out simulations using CHEMKIN-PRO[21] to simulate the shock waves experiment by Hong *et al.*[15] for H_2O_2

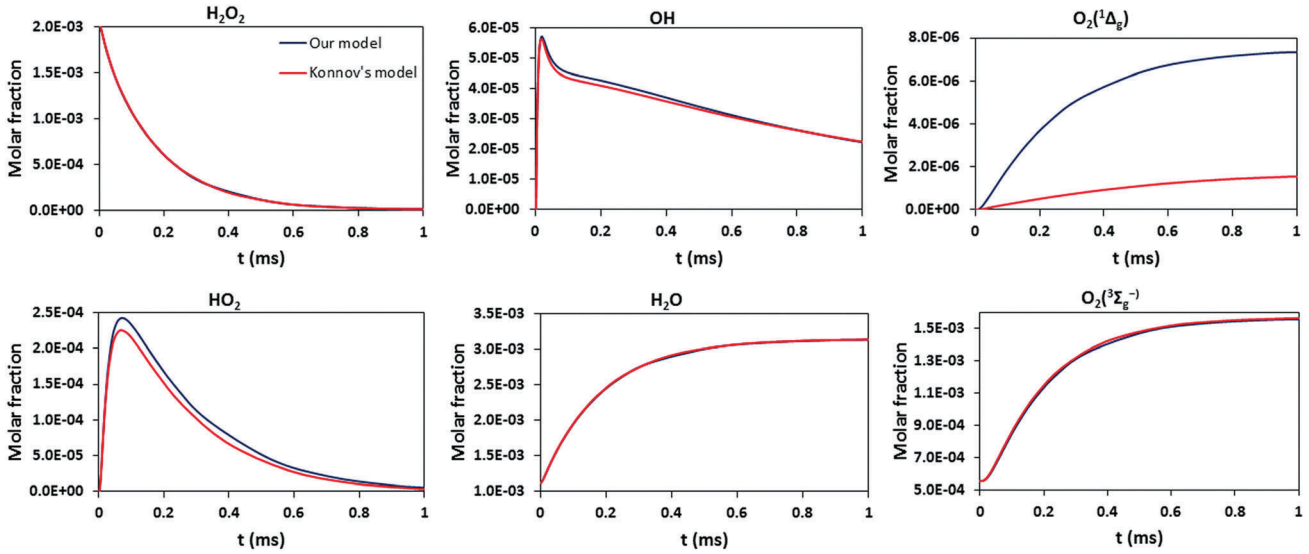

Fig. 5 Species concentration profiles for H_2O_2, OH, HO_2, H_2O, $O_2(^3\Sigma_g^-)$ and $O_2(^1\Delta_g)$ obtained in the shock waves simulations with CHEMKIN-PRO at 1182 K and 1.672 atm.

decomposition at 1182 K and 1.672 atm, as described in Section II.3.

First, we compare the results obtained in that simulation with Konnov's model and an updated model with our rate constants. Fig. 5 shows the species concentration profiles for H_2O_2, OH, HO_2, H_2O, $O_2(^3\Sigma_g^-)$ and $O_2(^1\Delta_g)$. Both models reproduce the concentration profiles for the OH and H_2O species obtained in Hong's reflected shock wave experiments (see Fig. 1 in ref. 15); both models also predict very similar results for H_2O_2, HO_2 and $O_2(^3\Sigma_g^-)$, but not for $O_2(^1\Delta_g)$, for which our updated model predicts a larger yield. At the end of the H_2O_2 decomposition process we predict a concentration of $O_2(^1\Delta_g)$ of 2.99 ppm, while Konnov's model predicts 0.70 ppm. These discrepancies in the yield of $O_2(^1\Delta_g)$ are due to the larger rate constants obtained in this work for the reaction $OH + HO_2 \rightarrow H_2O + O_2(^1\Delta_g)$, compared to those included in Konnov's model, which come from ref. 2 (see Table 3).

However, given that the rate constants for $OH + HO_2 \rightarrow H_2O + O_2(^3\Sigma_g^-)$ are significantly larger, the triplet channel is prominent, and we do not observe a significant amount of singlet oxygen when H_2O_2 decomposes. Thus, the H_2O_2 decomposition at 1182 K and 1.672 atm is not significantly affected when the new rate constants for $OH + HO_2 \rightarrow H_2O + O_2(^1\Delta_g)$ are included in the kinetic model developed by Konnov.[20] We performed the same simulations at 1000 K, 1500 K and 1800 K and observed no differences in the H_2O_2 decomposition using Konnov's and our rate constants.

The new reaction kinetics for $OH + HO_2 \rightarrow O_2(^3\Sigma_g^-)/O_2(^1\Delta_g)$ was also tested in the H_2–oxidizer mixtures specified in Section II.3 by predicting flame speeds and ignition delay times. The flame speeds and ignition delay times estimated with both models are included in the ESI.† Our findings show that the reaction $OH + HO_2 \rightarrow H_2O + O_2(^1\Delta_g)$ has a negligible effect on the combustion of H_2 unless the oxidizer is seeded with O_3, because the yield of $O_2(^1\Delta_g)$ may not be large enough to make a difference even at high temperatures. In mixtures with an oxidizer made of 60.9% $O_2(^3\Sigma_g^-)$ + 39.1% O_3 small differences appear in the flame speed predicted by both models, being that of our updated model slightly larger. However, large amounts of O_3 should be added to notice a small effect. As was pointed out by Konnov,[20] the reaction

$$H + HO_2 \rightarrow H_2 + O_2(^1\Delta_g) \qquad (R3)$$

with a rate constant at room temperature of $k(298\ K) = 1.2 \times 10^{-12}$ cm^3 molecule^{-1} s^{-1}, that is, much larger than that of the reaction $OH + HO_2 \rightarrow H_2O + O_2(^1\Delta_g)$ ($k(298\ K) = 1.1 \times 10^{-15}$ cm^3 molecule^{-1} s^{-1}), might be the main source of $O_2(^1\Delta_g)$, and very large [OH]/[H] ratios might be necessary for the reaction $OH + HO_2 \rightarrow H_2O + O_2(^1\Delta_g)$ to have a remarkable effect on the studied systems.

IV. Conclusions

By means of *ab initio* calculations at the W3X-L//CCSD = FC/cc-pVTZ level we have calculated the rate constants of the reactions $OH + HO_2 \rightarrow H_2O + O_2(^3\Sigma_g^-)/O_2(^1\Delta_g)$. Our results for $OH + HO_2 \rightarrow H_2O + O_2(^3\Sigma_g^-)$ using the microcanonical variational transition state theory are in good agreement with the most recent theoretical and experimental measurements by Burke *et al.*[7] and Hong *et al.*,[15] confirming the non-Arrhenius temperature dependence and the presence of a minimum in the rate constants at 850 K. This temperature dependence is due to the formation of a hydrogen-bonded intermediate complex located in the entry channel, which induces a change in the activation energy from negative at temperatures below 850 K to positive at higher temperatures. Due to its large rate constant values, the barrierless radical–radical reaction $OH + HO_2 \rightarrow H_2O + O_2(^3\Sigma_g^-)$ is expected to play a role in hydrogen combustion and atmospheric chemistry.

The rate constants for OH + HO_2 → H_2O + $O_2(^1\Delta_g)$ were calculated using the multistructural variational transition state theory. Our results improve the only set of data available for this reaction, reported by González *et al.*[2] by using lower level *ab initio* calculations, MP4/6-31G**, and a less sophisticated method to compute the rate constants and the tunneling contribution. We predict rate constants that are significantly larger than those predicted by González *et al.*[2]

The reaction on the triplet PES is energetically favored over the reaction on the singlet PES; there is about 2.5 kcal mol^{-1} difference in the barrier heights, resulting in very small branching ratios to the singlet channel even at high temperatures: 1.43% at 2000 K.

Using these rate constants we updated the kinetic model recently developed by Konnov,[20] which includes the rate constants from González *et al.*[2] (singlet channel) and Hong *et al.*[15] (triplet channel), to simulate the shock waves experiment by Hong *et al.*[15] for H_2O_2 decomposition using CHEMKIN-PRO. The model was also used to estimate flame speeds and ignition delay times of different H_2–oxidizer mixtures. We did not observe any effect of the reaction OH + HO_2 → H_2O + $O_2(^1\Delta_g)$ on the rate of the H_2O_2 decomposition compared to Konnov's model, even though we predict a larger yield of $O_2(^1\Delta_g)$; the effect is also negligible on the flame speeds and ignition delay times of the H_2 mixtures, unles the oxidizer is seeded with O_3. In this case, our model predicts slightly larger flame speeds.

We conclude that the reaction OH + HO_2 → H_2O + $O_2(^1\Delta_g)$ do not form enough singlet excited oxygen to play a remarkable role in these systems, and the reaction will primarily take place on the triplet PES. However, the new set of rate constants reported in this work for OH + HO_2 → H_2O + $O_2(^1\Delta_g)$ may be useful in other systems/simulations that are more sensitive to the presence of singlet excited oxygen, such as systems with ozone addition or plasma assisted combustion.[59–62]

Conflicts of interest

There are no conflicts to declare.

Acknowledgements

This work was supported by King Abdullah University of Science and Technology (KAUST), Office of Sponsored Research (OSR) under Award No. OSR-2016-CRG5-3022. The part of this work performed at the University of Missouri-Columbia, United States, was sponsored under grant number W911NF-14-1-0359 (U. S. Army Research Office). We thank the resources of the Supercomputing Laboratory at KAUST and the "Centro Extremeño de Investigación, Innovación Tecnológica y Supercomputación (CENITS)", Spain, for use of Lusitania supercomputer resources. We also acknowledge Prof. Donald L. Thompson for his valuable comments.

References

1 M. Monge-Palacios and H. Rafatijo, On the Role of the Termolecular Reactions $2O_2 + H_2 \rightarrow 2HO_2$ and $2O_2 + H_2 \rightarrow H + HO_2 + O_2$ in Formation of the First Radicals in Hydrogen Combustion: *Ab Initio* Predictions of Energy Barriers, *Phys. Chem. Chem. Phys.*, 2017, **19**, 2175–2185.

2 C. González, J. Theisen, L. Zhu, H. B. Schlegel, W. L. Hase and E. W. Kaiser, Kinetics of the Reaction between OH and HO_2 on the Singlet Potential Energy Surface, *J. Phys. Chem.*, 1992, **96**, 1767–1774.

3 M. Mozurkewich, Reactions of HO_2 with Free Radicals, *J. Phys. Chem.*, 1986, **90**, 2216–2221.

4 D. W. Toohey and J. G. Anderson, Theoretical Investigations of Reactions of Some Radicals with HO_2. 1. Hydrogen Abstractions by Direct Mechanism, *J. Phys. Chem.*, 1989, **93**, 1049–1058.

5 C. González, J. Theisen, H. B. Schlegel, W. L. Hase and E. W. Kaiser, Kinetics of the Reaction between OH and HO_2 on the Triplet Potential Energy Surface, *J. Phys. Chem.*, 1992, **96**, 1767–1774.

6 L. F. Keyser, Kinetics of the Reaction OH + HO_2 → H_2O + O_2 from 254 to 382 K, *J. Phys. Chem.*, 1988, **92**, 1193–1200.

7 M. P. Burke, S. J. Klippenstein and L. B. Harding, A Quantitative Explanation for the Apparent Anomalous Temperature Dependence of OH + HO_2 = H_2O + O_2 through Multi-scale Modelling, *Proc. Combust. Inst.*, 2013, **34**, 547–555.

8 E. E. Greenwald, S. W. North, Y. Georgievskii and S. J. Klippenstein, A Two Transition State Model for Radical-Molecule Reactions: a Case Study of the Addition of OH to C_2H_4, *J. Phys. Chem.*, 2005, **109**, 6031–6044.

9 Y. Georgievskii and S. J. Klippenstein, Strange Kinetics of the C_2H_6 + CN Reaction Explained, *J. Phys. Chem. A*, 2007, **111**, 3802–3811.

10 U. C. Sridharan, L. X. Qiu and F. Kaufman, Rate Constant of the OH + HO_2 Reaction from 252 to 420 K, *J. Phys. Chem.*, 1984, **88**, 1281–1282.

11 H. Hippler, H. Neunaber and J. Troe, Shock Wave Studies of the Reactions OH + H_2O_2 → H_2O + HO_2 and OH + HO_2 → H_2O + O_2 between 930 and 1680 K, *J. Chem. Phys.*, 1995, **103**, 3510–3516.

12 Ch. Kappel, K. Luther and J. Troe, Shock Wave Study of the Unimolecular Dissociation of H_2O_2 in its Falloff Range and of its Secondary Reactions, *Phys. Chem. Chem. Phys.*, 2002, **4**, 4392–4398.

13 N. K. Srinivasan, M. C. Su, J. W. Sutherland, J. V. Michael and B. Ruscic, Reflected Shock Tube Studies of High-Temperature Rate Constants for OH + NO_2 → HO_2 + NO and OH + HO_2 → H_2O + O_2, *J. Phys. Chem. A*, 2006, **110**, 6602–6607.

14 Z. Hong, S. S. Vasu, D. F. Davidson and R. K. Hanson, Experimental Study of the Rate of OH + HO_2 → H_2O + O_2 at High Temperatures Using the Reverse Reaction, *J. Phys. Chem. A*, 2010, **114**, 5520–5525.

15 Z. Hong, K. Y. Lam, R. Sur, S. Wang, D. F. Davidson and R. K. Hanson, On the Rate Constants of OH + HO_2 and HO_2 + HO_2: a Comprehensive Study of H_2O_2 Thermal Decomposition Using Multi-Species Laser Absorption, *Proc. Combust. Inst.*, 2013, **34**, 565–571.

16 J. J. Schwab, W. H. Brune and J. G. Anderson, Kinetics and Mechanism of the OH + HO_2 Reaction, *J. Phys. Chem.*, 1989, **93**, 1030–1035.

17 R. R. Lii, M. C. Gorse Jr. and S. G. Sauer Jr., Rate Constant for the Reaction of OH with HO_2, *J. Phys. Chem.*, 1980, **84**, 819–821.

18 R. A. Cox, J. P. Burrows and T. J. Wallington, Rate Coefficient for the Reaction OH + HO_2 = H_2O + O_2 at 1 Atmosphere Pressure and 308 K, *Chem. Phys. Lett.*, 1981, **84**, 217–221.

19 V. B. Rozenshtein, Y. M. Gershenzon, S. D. II'in and O. P. Kishkovitch, Reactions of HO_2 with NO, OH and HO_2 Studied by EPR/LMR Spectroscopy, *Chem. Phys. Lett.*, 1984, **112**, 473–478.

20 A. Konnov, On the Role Excited Species in Hydrogen Combustion, *Combust. Flame*, 2015, **162**, 3755–3772.

21 Reaction Design, Inc., CHEMKIN-PRO Release 15101, Reaction Design, Inc., San Diego, CA, 2010.

22 M. J. Frisch, G. W. Trucks, H. B. Schlegel, G. E. Scuseria, M. A. Robb, J. R. Cheeseman, G. Scalmani, V. Barone, B. Mennucci, G. A. Petersson, H. Nakatsuji, M. Caricato, X. Li, H. P. Hratchian, A. F. Izmaylov, J. Bloino, G. Zheng, J. L. Sonnenberg, M. Hada, M. Ehara, K. Toyota, R. Fukuda, J. Hasegawa, M. Ishida, T. Nakajima, Y. Honda, O. Kitao, H. Nakai, T. Vreven, J. A. Montgomery Jr., J. E. Peralta, F. Ogliaro, M. Bearpark, J. J. Heyd, E. Brothers, K. N. Kudin, V. N. Staroverov, R. Kobayashi, J. Normand, K. Raghavachari, A. Rendell, J. C. Burant, S. S. Iyengar, J. Tomasi, M. Cossi, N. Rega, J. M. Millam, M. Klene, J. E. Knox, J. B. Cross, V. Bakken, C. Adamo, J. Jaramillo, R. Gomperts, R. E. Stratmann, O. Yazyev, A. J. Austin, R. Cammi, C. Pomelli, J. W. Ochterski, R. L. Martin, K. Morokuma, V. G. Zakrzewski, G. A. Voth, P. Salvador, J. J. Dannenberg, S. Dapprich, A. D. Daniels, Ö. Farkas, J. B. Foresman, J. V. Ortiz, J. Cioslowski and D. J. Fox, *GAUSSIAN 09, Revision D.01*, Gaussian Inc., Wallingford, CT, 2009.

23 H. J. Werner, P. J. Knowles, G. Knizia, F. R. Manby, M. Schütz, P. Celani, T. Korona, R. Lindh, A. Mitrushenkov, G. Rauhut, K. R. Shamasundar, T. B. Adler, R. D. Amos, A. Bernhardsson, A. Berning, D. L. Cooper, M. J. O. Deegan, A. J. Dobbyn, F. Eckert, E. Goll, C. Hampel, A. Hesselmann, G. Hetzer, T. Hrenar, G. Jansen, C. Köppl, Y. Liu, A. W. Lloyd, R. A. Mata, A. J. May, S. J. McNicholas, W. Meyer, M. E. Mura, A. Nicklass, D. P. O'Neill, P. Palmieri, D. Peng, K. Pflüger, R. Pitzer, M. Reiher, T. Shiozaki, H. Stoll, A. J. Stone, R. Tarroni, T. Thorsteinsson and M. Wang, *MOLPRO, version 2012.1, A Package of ab initio Programs*.

24 M. Kallay, Z. Rolik, I. Ladjanszki, L. Szegedy, B. Ladoczki, J. Csontos and B. Kornis, MRCC, A Quantum Chemical Program Suite, http://www.mrcc.hu/.

25 J. Cížek, in *Advances in Chemical Physics*, ed. P. C. Hariharan, Wiley Interscience, New York, 1969, vol. 14.

26 T. H. Dunning Jr., Gaussian Basis Sets for Use in Correlated Molecular Calculations. I. The Atoms Boron through Neon and Hydrogen, *J. Chem. Phys.*, 1989, **90**, 1007–1023.

27 B. Chan and L. Radom, W2X and W3X-L: Cost-Effective Approximations to W2 and W4 with kJ mol^{-1} Accuracy, *J. Chem. Theory Comput.*, 2015, **11**, 2109–2119.

28 J. C. Corchado, Y.-Y. Chuang, E. L. Coitiño, B. A. Ellingson and D. G. Truhlar, *GAUSSRATE 9.5*, University of Minnesota, Minneapolis, 2007.

29 M. J. Frisch, G. W. Trucks, H. B. Schlegel, G. E. Scuseria, M. A. Robb, J. R. Cheeseman, J. A. Montgomery Jr., T. Vreven, K. N. Kudin, J. C. Burant, J. M. Millam, S. S. Iyengar, J. Tomasi, V. Barone, B. Mennucci, M. Cossi, G. Scalmani, N. Rega, G. A. Petersson, H. Nakatsuji, M. Hada, M. Ehara, K. Toyota, R. Fukuda, J. Hasegawa, M. Ishida, T. Nakajima, Y. Honda, O. Kitao, H. Nakai, M. Klene, X. Li, J. E. Knox, H. P. Hratchian, J. B. Cross, V. Bakken, C. Adamo, J. Jaramillo, R. Gomperts, R. E. Stratmann, O. Yazyev, A. J. Austin, R. Cammi, C. Pomelli, J. W. Ochterski, P. Y. Ayala, K. Morokuma, G. A. Voth, P. Salvador, J. J. Dannenberg, V. G. Zakrzewski, S. Dapprich, A. D. Daniels, M. C. Strain, O. Farkas, D. K. Malick, A. D. Rabuck, K. Raghavachari, J. B. Foresman, J. V. Ortiz, Q. Q. Cui, A. G. Baboul, S. Clifford, J. Cioslowski, B. B. Stefanov, G. Liu, A. Liashenko, P. Piskorz, I. Komaromi, R. L. Martin, D. J. Fox, T. Keith, M. A. Al-Laham, C. Y. Peng, A. Nanayakkara, M. Challacombe, P. M. W. Gill, B. Johnson, W. Chen, M. W. Wong, C. Gonzalez and J. A. Pople, *Gaussian 03, Revision C.02*, Gaussian Inc., Wallingford, CT, 2004.

30 J. C. Corchado, Y.-Y. Chuang, P. L. Fast, W.-P. Hu, Y.-P. Liu, G. C. Lynch, K. A. Nguyen, C. F. Jackels, A. Fernandez-Ramos, B. A. Ellingson, B. J. Lynch, V. S. Melissas, J. Villá, I. Rossi, E. L. Coitinño, J. Pu, T. V. Albu, R. Steckler, B. C. Garrett, A. D. Isaacson and D. G. Truhlar, *POLYRATE 9.5*, University of Minnesota, Minneapolis, 2007.

31 J. Zhen, J. L. Bao, R. Meana-Pañeda, S. Zhang, B. J. Lynch, J. C. Corchado, Y.-Y. Chuang, P. L. Fast, W.-P. Hu, Y.-P. Liu, G. C. Lynch, K. A. Nguyen, C. F. Jackels, A. F. Ramos, B. A. Ellingson, V. S. Melissas, J. Villa, I. Rossi, E. L. Coitiño, J. Pu, T. V. Albu, A. Ratkiewicz, R. Steckler, B. C. Garret, A. D. Isaacson and D. G. Truhlar, *POLYRATE2016-2A*, Univeristy of Minnesota, Minneapolis, 2016.

32 J. Zheng, S. L. Mielke, K. L. Clarkson, R. Meana-Pañeda and D. G. Truhlar, *MSTor, version 2013*, University of Minnesota, Minneapolis, 2013.

33 D. G. Truhlars, Variational Transition-State Theory, *Acc. Chem. Res.*, 1980, **13**, 440–448.

34 A. Fernández-Ramos, B. A. Ellingson, R. Meana-Pañeda, J. M. C. Marques and D. G. Truhlar, Symmetry Numbers and Chemical Reaction Rates, *Theor. Chem. Acc.*, 2007, **118**, 813–826.

35 J. Zheng, T. Yu, E. Papajak, I. M. Alecu, S. L. Mielke and D. G. Truhlar, Practical Methods for Including Torsional Anharmonicity in Thermochemical Calculations on Complex Molecules: The Internalcoordinate Multi-structural Approximation, *Phys. Chem. Chem. Phys.*, 2011, **13**, 10885–10907.

36 J. Zheng and D. G. Truhlar, Quantum Thermochemistry: Multistructural Method with Torsional Anharmonicity Based on a Coupled Torsional Potential, *J. Chem. Theory Comput.*, 2013, **9**, 1356–1367.

37 T. Yu, J. Zheng and D. G. Truhlar, Multi-structural Variational Transition State Theory. Kinetics of the 1,4-hydrogen

Shift Isomerization of the Pentyl Radical with Torsional Anharmonicity, *Chem. Sci.*, 2011, **2**, 2199–2213.

38 B. C. Garrett and D. G. Truhlar, Generalized Transition State Theory. Bond Energy-bond Order Method for Canonical Variational Calculations with Application to Hydrogen atom Transfer Reactions, *J. Am. Chem. Soc.*, 1979, **101**, 4534–4548.

39 D. G. Truhlar, A. D. Isaacson and B. C. Garrett, *Theory of Chemical Reaction Dynamics*, Boca Raton, FL, 1985, vol. 4, pp. 65–137.

40 H. E. Hunziker and H. R. Wendt, Near Infrared Absorption Spectrum of HO_2, *J. Chem. Phys.*, 1974, **60**, 4622.

41 K. H. Becker, E. H. Fink, P. Langen and U. Schurath, Near Infrared Emission Bands of the HO_2 Radical, *J. Chem. Phys.*, 1974, **60**, 4623–4625.

42 NIST Computational Chemistry Comparison and Benchmark Database, NIST Standard Reference Database Number 101 2016, ed. R. D. Johnson III, available at: http://cccbdb.nist.gov/.

43 D. h. Lu, T. N. Truong, V. S. Melissas, G. C. Lynch, Y. P. Liu, B. C. Garrett, R. Steckler, A. D. Isaacson, S. N. Rai, S. G. C. Hancock, G. C. Lauderdale, T. Joseph and D. G. Truhlar, POLYRATE 4: A New Version of a Computer Program for the Calculation of Chemical Reaction Rates for Polyatomics, *Comput. Phys. Commun.*, 1992, **71**, 235–262.

44 C. F. Jackels and D. H. Phillips, An *Ab Initio* Investigation of Possible Intermediates in the Reaction of the Hydroxyl and Hydroperoxyl Radicals, *J. Chem. Phys.*, 1986, **84**, 5013–5024.

45 T. Zhang, W. Wang, C. Li, Y. Du and J. Lu, Catalytic Effect of a Single Water Molecule on the Atmospheric Reaction of HO_2 + OH: Fact or Fiction? A Mechanistic and Kinetic Study, *RSC Adv.*, 2013, **3**, 7381–7391.

46 A. Starik and A. Sharipov, Theoretical Analysis of Reaction Kinetics with Singlet Oxygen Molecules, *Phys. Chem. Chem. Phys.*, 2011, **13**, 16424–16436.

47 V. E. Kozlov, A. M. Starik and N. S. Titova, Enhancement of Combustion of a Hydrogen-Air Mixture by Excitation of O_2 Molecules to the $a^1\Delta_g$ State, *Combust., Explos. Shock Waves*, 2008, **44**, 371–379.

48 A. M. Starik, N. S. Titova, L. V. Bezgin and V. I. Kopchenov, Control of Combustion by Generation of Singlet Oxygen Molecules in Electrical Discharge, *Czech. J. Phys.*, 2006, **56**, 1357–1363.

49 A. M. Starik, V. E. Kozlov and N. S. Titova, On Mechanisms of a Flame Velocity Increase upon Activation of O_2 Molecules in Electrical Discharge, *J. Phys. D: Appl. Phys.*, 2008, **41**, 125206.

50 V. V. Smirnov, O. M. Stelmakh, V. I. Fabelinsky, D. N. Kozlov, A. N. Starik and N. S. Titova, On the Influence of Electronically Excited Oxygen Molecules on Combustion of Hydrogen-Oxygen Mixture, *J. Phys. D: Appl. Phys.*, 2008, **41**, 192001.

51 K. Park, A. West, E. Raheja, B. Sellner, H. Lischka, T. L. Windus and W. L. Hase, Singlet and Triplet Potential Surfaces for the O_2 + C_2H_4 Reaction, *J. Chem. Phys.*, 2010, **133**, 184306.

52 B. Ruscic, R. E. Pinzon, M. L. Morton, G. von Laszewski, S. J. Bittner, S. G. Nijsure, K. A. Amin, M. Minkoff and A. F. Wagner, Introduction to Active Thermochemical Tables: Several "Key" Enthalpies of Formation Revisited, *J. Phys. Chem. A*, 2004, **108**, 9979–9997.

53 B. Ruscic, *Active Thermochemical Tables, In 2005 Yearbook of Science and Technology*, McGraw-Hill, New York, 2004.

54 B. Ruscic, R. E. Pinzon, G. von Laszewski, D. Kodeboyina, A. Burcat, D. Leahy, D. Montoya and A. F. Wagner, Active Thermochemical Tables: Thermochemistry for the 21st Century, *J. Phys.: Conf. Ser.*, 2005, **16**, 561–570.

55 M. W. Chase Jr., C. A. Davies, J. R. Downey Jr., D. J. Frurip, R. A. McDonald and A. N. Syverud, JANAF Thermochemical Tables, *J. Phys. Chem. Ref. Data*, 1985, **14**(suppl. 1), 1–383.

56 M. Monge-Palacios and J. Espinosa-García, Reaction-Path Dynamics Calculations of the Cl + NH_3 Hydrogen Abstraction Reaction: The Role of the Intermediate Complexes, *J. Phys. Chem. A*, 2010, **114**, 4418–4426.

57 M. Monge-Palacios, C. Rangel, J. C. Corchado and J. Espinosa-García, Analytical Potential Energy Surface for the Reaction with Intermediate Complexes NH_3 + Cl → NH_2 + HCl: Application to the Kinetics Study, *Int. J. Quantum Chem.*, 2012, **112**, 1887–1903.

58 J. I. Steinfeld, J. S. Francisco and W. L. Hase, *Chemical Kinetics and Dynamics*, Prentice Hall, New Jersey, 2nd edn, 1999.

59 A. A. Konnov, Modeling Ozone Decomposition Flames, *Energy Fuels*, 2013, **27**, 501–506.

60 K. F. Pliavaka, S. V. Gorbatov, S. V. Shushkou, F. V. Pliavaka, A. P. Chernukho, S. A. Zhdanok, V. V. Naumov, A. M. Starik, A. Bourig and J.-P. Martin, Singlet Oxygen Production in Electrical non-Self-Sustained HV Pulsed + DC Cross Discharge at Atmospheric Pressure with Application to Plasma Assisted Combustion Technologies, *Nonequilibrium Processes in Combustion and Plasma Based Technologies*, Minsk, 2006, pp. 186–191.

61 A. Bourig, D. Thevenin, J. P. Martin, G. Janiga and K. Zahringer, Numerical Modeling of H_2-O_2 Flames Involving Electronically-Excited Species $O_2(^1\Delta_g)$, $O(^1D)$ and $OH(^2\Sigma_g^+)$, *Proc. Combust. Inst.*, 2009, **32**, 3171–3179.

62 A. A. Chukalovsky, K. S. Klopovsky, M. A. Liberman, Yu. A. Mankelevich, N. A. Popov, O. V. Proshina and T. V. Rakhimova, Study of Singlet Delta Oxygen $O_2(^1\Delta_g)$ Impact on H_2–O_2 Mixture Ignition in Flow Reactor: 2D Modeling, *Combust. Sci. Technol.*, 2012, **184**, 1768–1786.

